Attitude Control of a 3-DoF Quadrotor Platform using a Linear Quadratic Integral Differential Game Approach

Abstract

In this study, a linear quadratic integral differential game approach is applied to regulate and track the Euler angles for a quadrotor experimental platform using two players. One produces commands for each channel of the quadrotor and another generates the worst disturbance based on the mini-maximization of a quadratic criterion with integral action. For this purpose, first, the attitude dynamics of the platform are modeled and its parameters are identified based on the Nonlinear Least Squares Trust-Region Reflective method. The performance of the proposed controller is evaluated for regulation and tracking problems. The ability of the controller is also examined in the disturbance rejection. Moreover, the influence of uncertainty modeling is studied on the obtained results. Then, the performance of the proposed controller is compared with the classic Proportional Integral Derivative, Linear Quadratic Regulator, and Linear Quadratic Integral Regulator. The results demonstrate the effectiveness of the Game Theory on the Linear Quadratic Regulator approach when the input disturbance occurs.

Keywords:
Linear Quadratic Controller, Differential Game Theory, Quadrotor, 3-DoF Experimental Platform, Attitude Control.

1. Introduction

Quadrotors are a type of Vertical Unmanned Aerial Vehicle (VUAV), that have various applications such as investigation, strategic operation, optical sensing, and entertainment. The safe flight of the quadrotor in the presence of disturbances and mismodelling errors relies on a precise Attitude Control System (ACS). To regulate the quadrotor attitude, a Proportional Integral Derivative (PID) controller is utilized in [1, 5]. Due to the nonlinearity dynamics of the quadrotor, the PID strategy is not effective in the presence of disturbance and modeling error. To provide a faster control command in facing the modeling error and reduce the disturbance effect in the attitude control, the approaches such as Active Disturbance Rejection Control (ADRC) [8], nonlinear, and robust [10, 9] techniques can be found in the literatures. ADRC is a model-free control technique used for systems with disturbances and unknown dynamics. In ref [31], ADRC method and a robust U-model active disturbance rejection control (RUADRC) have been proposed to reduce the phase lag and enhance the disturbance rejection ability.

In the nonlinear control category, a Sliding Mode Control (SMC) [20, 23] law is applied based on the mathematical model of the plant and adopted for parameters perturbations. Moreover, this strategy is able to eliminate the disturbances of the system related to its high-gain feedback [35]. In refs [32], SMC method has been implemented to solve the nonlinear tracking problem for attitude control of the quadrotor, while the mismodelling error including time-varying mass has been considered. Moreover, in another strategy of nonlinear control, the intelligent approaches such as Reinforcement Learning (RL) [16, 21], iterative learning [14], neural network [17], and fuzzy logic [15] have also been employed to control the attitude of the quadrotor. Besides, reinforcement learning has been utilized to train the control policy for the attitude of the quadrotor when the disturbance occurs [30].

The robust control strategy explicitly deals with parameters or disturbances. The robust algorithms can be categorized into two approaches: robust methods and robust control structures. The robust methods are utilized in linear and nonlinear control systems to achieve robust stability and/or performance in the presence of bounded modelling errors. In ref [22], a Robust-PID strategy has been utilized to control the attitude dynamics of the quadrotor in presence of the aerodynamic disturbances like wind. In another approach such as H_∞ [29, 24] and μ-synthesis [25], a minimaximization of the cost function including control effort and regulation performance have been utilized to produce the angular velocity commands for the attitude dynamics of the quadrotor while a worst-case scenario related to maximum uncertainty and disturbance is considered.

In contrast with the policy of the robust control structure, the optimal control categories such as Linear Quadratic Gaussian (LQG) [36], Linear Quadratic Regulator (LQR) [3], Linear Quadratic Integral Regulator (LQIR) [4], and Model Predictive Controller (MPC) [26, 28] have been utilized to produce the optimal control commands for a quadrotor without considering the disturbance. Several methods with adding robust technique including Robust-LQR [11], Robust-LQG [33], Robust-MPC [34] and LQR-SMC can be found in the literature to reduce the disturbance effect. In another approach, the game theory technique is added to optimal control categories to provide a mathematical framework for analyzing decision-making in the presence of disturbance and modeling error. In this method, the control signals are produced using a pursuit-evasion game as well as the interactions and conflicts between two players are considered. The first player produces the control commands, and another player generates the worst disturbance based on the optimization of the desired objectives. An example of this category is the Linear Quadratic Regulator-Differential Game (LQR-DG) controller. The LQR-DG controller is implemented on a model of the ship [37].

The implementation of the optimal control category based on the game theory still does not exist in any of the previous works. In this study, an LQR-DG method with an integral action is implemented as real-time on the 3-DoF experimental platform of the quadrotor to produce the robust control commands, i.e., rotational velocity of the quadrotor. Since this control strategy is a model-based method, first, the experimental platform of the quadrotor is modeled using the Newton-Euler formulation and its linear state-space form is derived. Then, the parameters of the quadrotor are estimated by matching experimental data with results from the model simulation. In the next step, the proposed controller is implemented on the Arduino Mega2560 board using the embedded coder platform in MATLAB and its performance is investigated in regulation and tracking problems. Moreover, the rejection capability of the input disturbance and modeling error is tested. Finally, a comparison is also performed between the results of classical PID, LQR, and LQIR with the proposed method. Moreover, the performance of the proposed structure has been investigated in flight and compared to the robust controller structures including ADRC and Disturbance Observer-Based Control (DOBC). The results demonstrate that this method has an excellent performance in the attitude control of the quadrotor platform. A demo video of the results is available online here.

The innovation of this study mainly includes the following two aspects: (1) Proof of the proposed optimal-robust structure without steady-state error; For this purpose, first, the problem of an optimal control category based on the game theory approach with two players, one player tracks the best command, and the second player generates the input disturbance, is converted to the robust control problems. Then, an action integral is added to the linear quadratic regulator based on the game theory to eliminate the steady-state errors. Finally, proof of the proposed controller scheme based on the integral action is presented. (2) Implementation of the proposed optimal-robust structure; For this purpose, an optimal control strategy with integral action based on differential game theory is implemented on a 3-DOF quadrotor experimental setup. Then, the parameters of a quadrotor experimental setup have been identified with the experimental results. The performance of the proposed structure has been evaluated in flight and compared to the robust controller structures. Finally, the rejection capability of the input disturbance and modeling error is evaluated successfully.

This research is organized as follows: section 2 presents the problem statement. In section 3, the dynamic platform is modeled. Then, the presented controller architecture is denoted in section 4. In sections 5 and 6, numerical results and a conclusion are represented, respectively.

2. Problem Statement

The experimental quadrotor platform rotates freely with rotational velocity $(\Omega_i, i = 1, 2, 3, 4)$ about its roll, pitch, and yaw axes, according to Figure 1. The angular velocities in the body frame (p, q, r) and the Euler angles (ϕ, θ, ψ) are measured using an Attitude Heading Reference System (AHRS). The measured states are utilized in the structure of the proposed controller to stabilize the quadrotor platform. The graphical abstract of the LQIR-DG controller strategy is depicted in Figure 2.

Figure 1: 3-DoF Quadrotor platform.

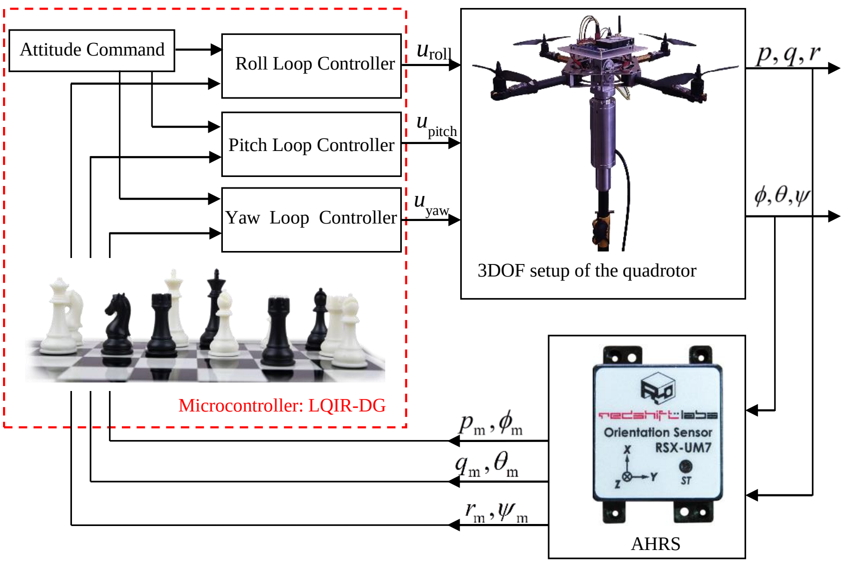

Figure 2: Graphical abstract of the LQIR-DG controller.

3. Model of the Quadrotor Platform

Here, the quadrotor platform is modeled as nonlinear. Then, a state-space model and a linear model are developed for control purposes to be utilized in the controller strategy. Finally, a nonlinear identification method is applied to identify the parameters of the quadrotor.

3.1. Quadrotor Configuration

According to Figure3, the 3-DoF quadrotor schematic is including four rotors rotating the z_B axis in the body frame with a rotational velocity, Ω_i $(i = 1, 2, 3, 4)$. To eliminate the yawing moment, rotors (2, 4) and (1, 3) rotate clockwise and counter counterclockwise, respectively.

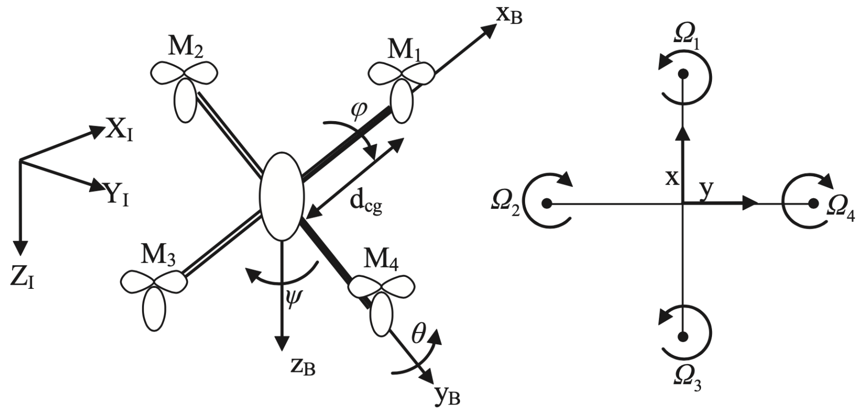

Figure 3: Quadrotor configuration.

3.2. Dynamic Modeling of the Quadrotor Platform

Here, according to Newton-Euler, the model of the quadrotor platform is presented as follows [7, 6]:

$$\dot{p} = \Gamma_1 pq - \Gamma_2 qr + \Gamma_3 \mathrm{bd_{cg}}(\Omega_{c,2}^2 - \Omega_{c,4}^2) + \Gamma_4 \mathrm{d}(\Omega_{c,1}^2 - \Omega_{c,2}^2 + \Omega_{c,3}^2 - \Omega_{c,4}^2) + \Gamma_5 q \Omega_{c,r} + \Gamma_3 d_{\mathrm{roll}} + \Gamma_4 d_{\mathrm{yaw}} \quad (1)$$

$$\dot{q} = \Gamma_6 pr - \Gamma_7 (p^2 - r^2) + \Gamma_8 \mathrm{bd_{cg}}(\Omega_{c,1}^2 - \Omega_{c,3}^2) + \Gamma_9 p \Omega_{c,r} + \Gamma_8 d_{\mathrm{pitch}} \quad (2)$$

$$\dot{r} = \Gamma_{10} pq - \Gamma_1 qr + \Gamma_{11}(\Omega_{c,1}^2 - \Omega_{c,2}^2 + \Omega_{c,3}^2 - \Omega_{c,4}^2) + \Gamma_4 \mathrm{bd_{cg}}(\Omega_{c,2}^2 - \Omega_{c,4}^2) + \Gamma_{11} d_{\mathrm{roll}} + \Gamma_4 d_{\mathrm{yaw}} \quad (3)$$

In the above equations, $\Gamma_i (i = 1, \ldots, 8)$ is defined as

$$\begin{aligned}
&\Gamma_1 = \frac{\mathrm{I_{xz}}\left(\mathrm{I_{xx}} - \mathrm{I_{yy}} + \mathrm{I_{zz}}\right)}{\Gamma}, && \Gamma_2 = \frac{\mathrm{I_{zz}}\left(\mathrm{I_{zz}} - \mathrm{I_{yy}}\right) + \mathrm{I_{xz}^2}}{\Gamma}, && \Gamma_3 = \frac{\mathrm{I_{zz}}}{\Gamma}, \quad \Gamma_4 = \frac{\mathrm{I_{xz}}}{\Gamma}\\
&\Gamma_5 = \frac{\mathrm{I_{rotor}}}{\mathrm{I_{xx}}}, && \Gamma_6 = \frac{\mathrm{I_{zz}} - \mathrm{I_{xx}}}{\mathrm{I_{yy}}}, && \Gamma_7 = \frac{\mathrm{I_{xz}}}{\mathrm{I_{yy}}}, \quad \Gamma_8 = \frac{1}{\mathrm{I_{yy}}}\\
&\Gamma_9 = \frac{\mathrm{I_{rotor}}}{\mathrm{I_{yy}}}, && \Gamma_{10} = \frac{\left(\mathrm{I_{xx}} - \mathrm{I_{yy}}\right) + \mathrm{I_{xz}^2}}{\Gamma}, && \Gamma_{11} = \frac{\mathrm{I_{xx}}}{\Gamma}
\end{aligned} \quad (4)$$

Moreover $\Gamma = \mathrm{J_x J_z} - \mathrm{J_{xy}^2}$. where $\Omega_{c,i}$ $(i = 1, 2, 3, 4)$ is the rotational velocity, computed as

$$\Omega_{c,1}^2 = \Omega_{\mathrm{mean}}^2 + \frac{1}{2\mathrm{b}\,\mathrm{d_{cg}}} u_{\mathrm{pitch}} + \frac{1}{4d} u_{\mathrm{yaw}} \quad (5)$$

$$\Omega_{c,2}^2 = \Omega_{\mathrm{mean}}^2 + \frac{1}{2\mathrm{b}\,\mathrm{d_{cg}}} u_{\mathrm{roll}} - \frac{1}{4d} u_{\mathrm{yaw}} \quad (6)$$

$$\Omega_{c,3}^2 = \Omega_{\mathrm{mean}}^2 - \frac{1}{2\mathrm{b}\,\mathrm{d_{cg}}} u_{\mathrm{pitch}} + \frac{1}{4d} u_{\mathrm{yaw}} \quad (7)$$

$$\Omega_{c,4}^2 = \Omega_{\mathrm{mean}}^2 - \frac{1}{2\mathrm{b}\,\mathrm{d_{cg}}} u_{\mathrm{roll}} - \frac{1}{4d} u_{\mathrm{yaw}} \quad (8)$$

In the above equation, Ω_{mean} is the rotational velocity of the rotors. Also, $\mathrm{d_{cg}}$, d, and b represent the distance between the rotors and the gravity center, drag factor, and thrust factor, respectively. d_{roll}, d_{pitch}, and d_{yaw} denote the disturbances produced in the body coordinate frame. Additionally, u_{roll}, u_{pitch}, and u_{yaw} are control commands generated by the LQIR-DG controller. $\mathrm{I_{xx}}$, $\mathrm{I_{yy}}$, and $\mathrm{I_{zz}}$ are the moments of inertia. Euler angle rates are also determined from angular body rates as follows:

$$\begin{bmatrix} \dot{\phi} \\ \dot{\theta} \\ \dot{\psi} \end{bmatrix} = \begin{bmatrix} 1 & \sin(\phi)\tan(\theta) & \cos(\phi)\tan(\theta) \\ 0 & \cos(\phi) & -\sin(\phi) \\ 0 & \sin(\phi)/\cos(\theta) & \cos(\phi)/\cos(\theta) \end{bmatrix} \begin{bmatrix} p \\ q \\ r \end{bmatrix} \tag{9}$$

3.3. State-Space Formulation

By defining $\mathbf{x}_{\text{roll}} = \begin{bmatrix} x_1 & x_2 \end{bmatrix}^{\mathrm{T}} = \begin{bmatrix} p & \phi \end{bmatrix}^{\mathrm{T}}$, $\mathbf{x}_{\text{pitch}} = \begin{bmatrix} x_3 & x_4 \end{bmatrix}^{\mathrm{T}} = \begin{bmatrix} q & \theta \end{bmatrix}^{\mathrm{T}}$, and $\mathbf{x}_{\text{yaw}} = \begin{bmatrix} x_5 & x_6 \end{bmatrix}^{\mathrm{T}} = \begin{bmatrix} r & \psi \end{bmatrix}^{\mathrm{T}}$, as well as by considering the control inputs as $\boldsymbol{u} = \begin{bmatrix} u_{\text{roll}} & u_{\text{roll}} & u_{\text{roll}} \end{bmatrix} = \begin{bmatrix} \mathrm{b\,d_{cg}}(\Omega_{c,2}^2 - \Omega_{c,4}^2) & \mathrm{b\,d_{cg}}(\Omega_{c,1}^2 - \Omega_{c,3}^2) & \mathrm{b\,d_{cg}}(\Omega_{c,1}^2 - \Omega_{c,2}^2 + \Omega_{c,3}^2 - \Omega_{c,4}^2) \end{bmatrix}$. The nonlinear model of the quadrotor platform in the state-space form $\dot{\boldsymbol{x}} = \boldsymbol{f}(\boldsymbol{x}, \boldsymbol{u})$ is presented as follows:

$$f_1 = \dot{x}_1 = \Gamma_1 x_1 x_3 - \Gamma_2 x_3 x_5 + \Gamma_3(u_{\text{roll}} + d_{\text{roll}}) + \Gamma_4(u_{\text{yaw}} + u_{\text{yaw}}) + \Gamma_5 x_3 \Omega_{c,r} \tag{10}$$

$$f_2 = \dot{x}_2 = x_1 + (x_3 \sin(x_2) + x_5 \cos(x_2)) \tan(x_4) \tag{11}$$

$$f_3 = \dot{x}_3 = \Gamma_6 x_1 x_5 - \Gamma_7(x_1^2 - x_5^2) + \Gamma_8(u_{\text{pitch}} + d_{\text{pitch}}) - \Gamma_9 x_1 \Omega_{c,r} \tag{12}$$

$$f_4 = \dot{x}_4 = x_3 \cos(x_2) - x_5 \sin(x_2) \tag{13}$$

$$f_5 = \dot{x}_5 = \Gamma_{10} x_1 x_3 - \Gamma_1 x_3 x_5 + \Gamma_{11}(u_{\text{yaw}} + d_{\text{yaw}}) + \Gamma_4(u_{\text{roll}} + d_{\text{roll}}) \tag{14}$$

$$f_6 = \dot{x}_6 = \frac{x_3 \sin(x_2) + x_5 \cos(x_2)}{\cos(x_4)} \tag{15}$$

The measurement vector, obtained from the AHRS, is presented as follows:

$$\mathbf{z} = \begin{bmatrix} p \; q \; r \; \phi \; \theta \; \psi \end{bmatrix}^{\mathrm{T}} + \boldsymbol{\nu} \tag{16}$$

where $\boldsymbol{\nu}$ is a Gaussian white noise. Moreover, the superscripts T indicate the transpose notation.

3.4. Linear Model

By defining $\dot{\mathbf{x}} = \begin{bmatrix} \dot{\mathbf{x}}_{\text{roll}} & \dot{\mathbf{x}}_{\text{pitch}} & \dot{\mathbf{x}}_{\text{yaw}} \end{bmatrix}^{\mathrm{T}}$, the linear model of the quadrotor platform represented about the equilibrium points ($\mathbf{x}_e^* = 0$ and $\mathbf{u}_e^* = 0$) as

$$\dot{\mathbf{x}} = \mathbf{A}\,\mathbf{x} + \mathbf{B}\,(\mathbf{u} + \mathbf{d}) \tag{17}$$

where $\mathbf{d} = \text{diag}([d_{\text{roll}}, d_{\text{pitch}}, d_{\text{yaw}}])$ denotes the input disturbance. $\mathbf{A}$ is the dynamic system matrix, denoted as

$$\mathbf{A} = \begin{bmatrix} \mathbf{A}_{\text{roll}} & \mathbf{0} & \mathbf{0} \\ \mathbf{0} & \mathbf{A}_{\text{pitch}} & \mathbf{0} \\ \mathbf{0} & \mathbf{0} & \mathbf{A}_{\text{yaw}} \end{bmatrix} \tag{18}$$

$\mathbf{A}_{\text{roll}} = \mathbf{A}_{\text{pitch}} = \mathbf{A}_{\text{yaw}} = \begin{bmatrix} 0 & 0 \\ 1 & 0 \end{bmatrix}$. Also, $\mathbf{B}$ is the input matrix defined as

$$\mathbf{B} = \begin{bmatrix} \Gamma_3 & 0 & \Gamma_4 \\ 0 & 0 & 0 \\ 0 & \Gamma_8 & 0 \\ 0 & 0 & 0 \\ \Gamma_4 & 0 & \Gamma_{11} \\ 0 & 0 & 0 \end{bmatrix} \tag{19}$$

3.5. Identification of the Platform Parameters

In this section, the Nonlinear Least Squares (NLS) algorithm is utilized for estimating the model parameters ($\mathbf{\Gamma}$) of the 3-DoF experimental platform using experimental data. This technique is based on the Trust-Region Reflective (TRR) method, which finds the best values for $\mathbf{\Gamma}$ by minimizing a cost function, defined as

$$\min_{\Gamma} \left(\| e(\Gamma) \|^2\right) = \min_{\Gamma} \left(\sum_{j=1}^{n} (\boldsymbol{z}_j - \tilde{\boldsymbol{z}}_j)(\boldsymbol{z}_j - \tilde{\boldsymbol{z}}_j)^{\mathrm{T}} \right) \tag{20}$$

where $\boldsymbol{z}$ and $\tilde{\boldsymbol{z}}$ are the experimental and simulated output signals when the same input signals are applied. Moreover, n is the number of scenarios. To find a vector Γ, the optimization process performs until convergence is achieved. The structure of the identification approach is illustrated in figure 4.

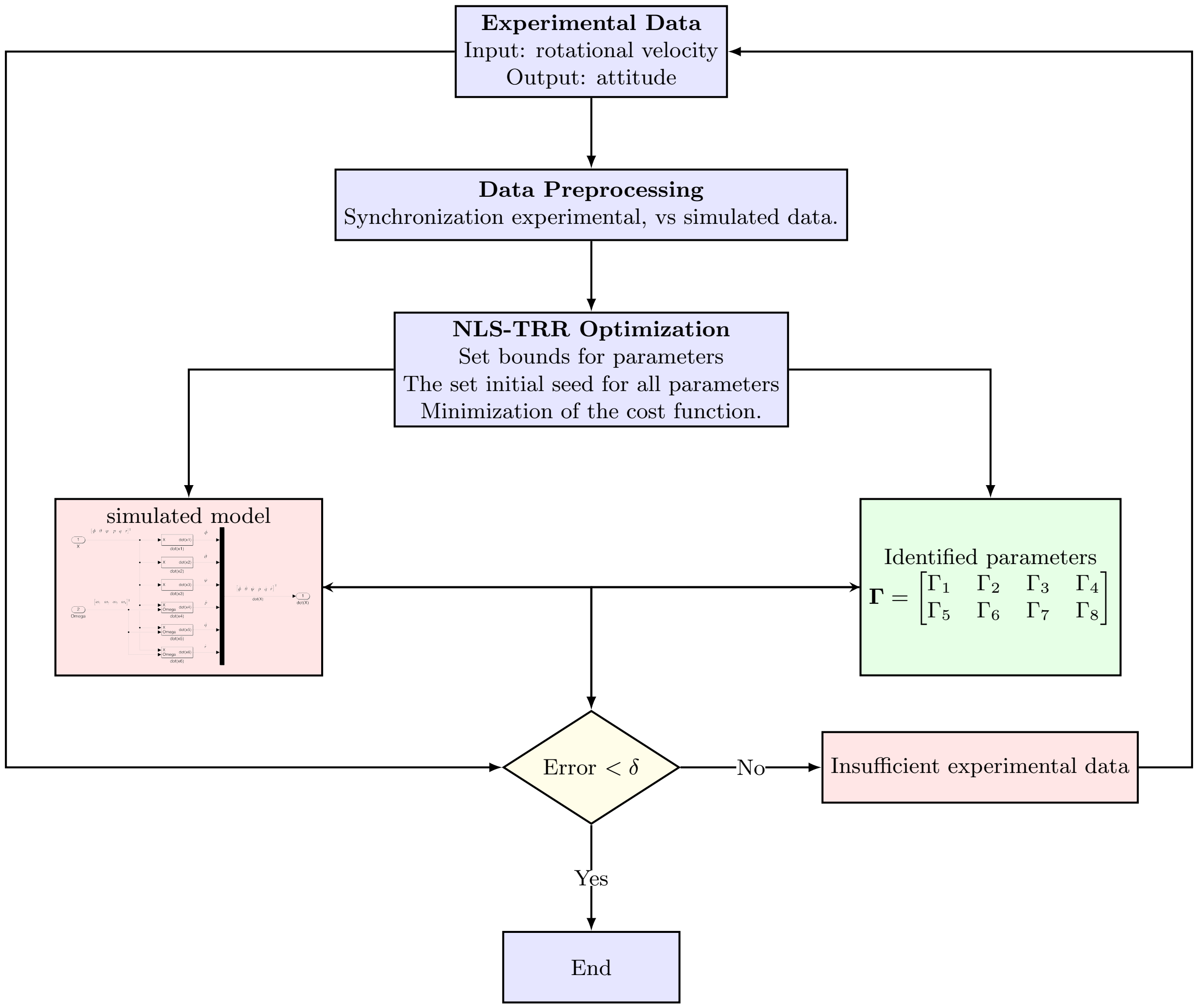

Figure 4: Structure of TRRLS identification approach.

4. LQIR-DG Controller Structure

First, the augmented states of the quadrotor platform, including the states and their integrals are selected to use in the structure of the LQIR-DG controller for eliminating the steady-state errors. Then, the design methodology of the controller structure is introduced to produce the best commands for the 3-DoF quadrotor platform.

4.1. Augmented States

To augment an integral action into the control strategy architecture, the augmented states are defined as $\mathbf{x}_a = \begin{bmatrix} \mathbf{x} & \int \mathbf{x} \end{bmatrix}^{\mathrm{T}}$. Then, the quadrotor platform model, utilized in the controller structure, is presented as

$$\dot{\mathbf{x}}_a = \mathbf{A}_a \mathbf{x}_a + \mathbf{B}_a \left(\mathbf{u} + \mathbf{d} \right) \tag{21}$$

where $\mathbf{A}_a = \begin{bmatrix} \mathbf{A} & \mathbf{0} \\ \mathbf{I} & \mathbf{0} \end{bmatrix}$ and $\mathbf{B}_a = \begin{bmatrix} \mathbf{B} \\ \mathbf{0} \end{bmatrix}$. The notation $\mathbf{I}$ denotes the identity matrix.

4.2. LQIR-DG Control Scheme with Integral Action

In the proposed controller scheme, two fundamental players are selected in accordance with the game theory approach. The primary player determines the control commands, while another player generates the worst possible disturbance. To achieve the primary objective, the first player minimizes the following cost function but the other player maximizes it:

$$\min_u \max_d J(\mathbf{x}_{\mathrm{a}_i}, d_i, u_i) = \min_d \max_u \int_0^{\mathrm{t_f}} \left(\mathbf{x}_{\mathrm{a}_i}^{\mathrm{T}} \mathbf{Q}_i \mathbf{x}_{\mathrm{a}_i} + u_i^{\mathrm{T}} R u_i - d_i^{\mathrm{T}} R_d d_i \right) \mathrm{d}t \tag{22}$$

where $\mathrm{t_f}$ is the stop time and i-index denotes the roll, pitch, and yaw channels of the quadrotor. $\mathbf{Q_i}$, R_d, and R are weight coefficients of the cost function. By solving the above problem, the optimal control command is computed as follows [13]:

$$u_i = -\mathbf{K}_i \mathbf{x}_{\mathrm{a}_i} \tag{23}$$

Moreover, the worst disturbance is obtained as

$$d_i = \mathbf{K}_{\mathrm{d}_i} \mathbf{x}_{\mathrm{a}_i} \tag{24}$$

Here, $\mathbf{K_{d_i}}$ and $\mathbf{K_i}$ are gain values defined as follows:

$$\mathbf{K}_{\mathrm{d}_i} = R_d^{-1} \mathbf{B}_{\mathrm{a}_i}^{\mathrm{T}} \mathbf{P}_{\mathrm{a}_i} \tag{25}$$

$$\mathbf{K}_i = R^{-1} \mathbf{B}_{\mathrm{a}_i}^{\mathrm{T}} \mathbf{P}_{\mathrm{a}_i} \tag{26}$$

$\mathbf{P}_{\mathrm{a}_i}$ satisfy

$$-\mathbf{A}^{\mathrm{T}} \mathbf{P}_{\mathrm{a}_i} - \mathbf{P}_{\mathrm{a}_i} \mathbf{A} + \mathbf{P}_{\mathrm{a}_i} (\mathbf{S}_{\mathrm{a}_i} - \mathbf{S}_{\mathrm{a_d}_i}) \mathbf{P}_{\mathrm{a}_i} - \mathbf{Q}_i = 0 \tag{27}$$

where $\mathbf{S}_{\mathrm{a}_i} = \mathbf{B}_{\mathrm{a}_i} R^{-1} \mathbf{B}_{\mathrm{a}_i}^{\mathrm{T}}$ and $\mathbf{S}_{\mathrm{a_d}_i} = \mathbf{B}_{\mathrm{a}_i} R_d^{-1} \mathbf{B}_{\mathrm{a}_i}^{\mathrm{T}}$

5. Results

The results of the parameter identification and the LQIR-DG Controller for the quadrotor platform are presented. First, the quadrotor parameters are estimated based on the NLS method. Then, the performance of the LQIR-DG structure is evaluated. Table 1 presents the quadrotor and LQIR-DG parameters, respectively.

Table 1: Parameters of the Quadrotor Setup

Parameter	Unit	Value	Description
m_{total}	kg	1.074	Total Mass
d	$N.m.\sec^2/\text{rad}^2$	3.2×10^{-6}	Drag Factor
b	$N.\sec^2/\text{rad}^2$	3.13×10^{-5}	Thrust Factor
d_{cg}	m	0.2	CG Distance
Ω_{mean}	rpm	2000	Mean Rotor Speed
I_{xx}	$kg.m^2$	0.02839	Inertia about X-axis
I_{yy}	$kg.m^2$	0.03066	Inertia about Y-axis
I_{zz}	$kg.m^2$	0.0439	Inertia about Z-axis
I_{rotor}	$kg.m^2$	4.4398×10^{-5}	Rotor Inertia
I_{xz}	$kg.m^2$	6.87×10^{-7}	Inertia about XZ-axis

5.1. Setting of the LQIR-DG controller parameters

The parameters of the LQIR-DG controller approach, including weight coefficients ($\mathbf{Q}_i$ for i = roll, pitch, yaw, R_d, and R) are tuned using a heuristic optimization algorithm including the Tabu Continuous Ant Colony System (TCACS) [18] approach. In this method, ants utilize the concepts of promising lists and tabu balls to move toward the goal of ants gradually. The pseudocode of TCACS is shown in Algorithm 1. For this purpose, ants find promising areas to contain the global minimum and perform searching within tabu balls of the bad regions. TCACS parameters are shown in Table 2. Here, it is assumed that the value of R is identical for all attitude channels and considered with the value of 1. Moreover, the initial values of the ants position ($\mathbf{Q}_{\text{roll}}, \mathbf{Q}_{\text{pitch}}, \boldsymbol{Q}_{\text{yaw}}$ and R_d) for $l = 1, \ldots, N$ is selected using a random distribution. The cost is denoted in iteration i using the quality of the tracking error between the set-point, $\mathbf{x}_{sp}$, and the quadrotor states, $\boldsymbol{x} = \begin{bmatrix}\boldsymbol{x}_{\text{roll}} & \boldsymbol{x}_{\text{pitch}} & \boldsymbol{x}_{\text{yaw}}\end{bmatrix}^{\mathrm{T}}$ as

$$c = \int_0^{t_f} t\left(\boldsymbol{x}_{sp} - \boldsymbol{x}\right)^{\mathrm{T}}\left(\boldsymbol{x}_{sp} - \boldsymbol{x}\right)\, dt \tag{28}$$

where t and t_f are the response time of the system and the final time, respectively. Finally, when the stopping condition of the TCACS algorithm is reached, the best values of the LQIR-DG parameters are computed, shown in Table 3.

Algorithm 1 Pseudo-code of the TCACS optimization algorithm [18].

```
procedure TCACS
    Initialize parameters, lists, and values
    while not terminated do
        if first iteration then
            Sample initial ant positions
        else
            Move ants
        end if
        Update structures and distributions
    end while
end procedure
```

Table 2: Parameters of the TCACS optimization algorithm.

Parameter	Value	Description
N	15	Number of Ants
I_{max}	10000	Maximum of Iteration
Tolerance	10^{-4}	Maximum accepted error

Table 3: Optimal Values of the LQIR-DG controller parameters

Channel	Weighting Matrix	Values
Roll	$\mathbf{Q_{roll}}$	$\mathrm{diag}([0.02, 65.96, 83.04, 0.00])$
Pitch	$\mathbf{Q_{pitch}}$	$\mathrm{diag}([435.01, 262.60, 262.60, 0.00])$
Yaw	$\mathbf{Q_{yaw}}$	$\mathrm{diag}([4 \times 10^{-4}, 0.00, 0.133, 0])$
-	R_d	1.2764

5.2. Identification of the 3-DoF quadrotor platform model

As described in section 3.3, the parameters of the quadrotor platform, denoted by $\Gamma_i (i = 1, \ldots, 11)$, are identified using the NLS-TRR algorithm. To increase the accuracy of parameter identification, three scenarios are considered according to Table 4. In the first scenario, depicted in Figure 5, the quadrotor rotates about only one axis (roll, pitch, or yaw axes) to identify the parameters Γ_3, Γ_5, Γ_8, Γ_9, and Γ_{11}. In the second scenario, according to Figure 6, the parameters Γ_1 and Γ_7 are estimated by rotating the experimental platform around its roll and pitch axes simultaneously. Finally, Figure 7 displays the results of the third scenario including the estimation of the parameters Γ_2, Γ_4, Γ_6, and Γ_{10} for the UAV model, when the platform freely rotates around three axes. After the termination condition is met, the optimal values of the quadrotor parameters are computed and denoted in Table 5. These results illustrate that the outputs of the simulation results for the quadrotor model are consistent with reality.

Table 4: Scenarios for identification of quadrotor parameters.

Scenario	Description	Initial Condition (deg)			Rotational Velocity Commands (rpm)			
		ϕ_0	θ_0	ψ_0	Ω_1	Ω_2	Ω_3	Ω_4
I	roll free	38	-	-	2000	2000	2000	3400
	pitch free	-	-15	-	3700	2000	2000	2000
	yaw free	-	-	-75	2000	3300	2000	3300
II	roll & pitch free	8	-5	-	1700	3800	2400	1700
III	roll, pitch, & yaw free	8	-3	-146	1700	3800	2400	1700

Table 5: True values of the quadrotor parameters.

Parameter 1	Value 1	Parameter 2	Value 2	Parameter 3	Value 3
Γ_1	4.9895×10^{-6}	Γ_2	0.0029	Γ_3	42.1805
Γ_4	0.0002	Γ_5	-0.0023	Γ_6	2.5294
Γ_7	0.0002	Γ_8	18.46	Γ_9	0.0022
Γ_{10}	-1.4456×10^{-5}	Γ_{11}	24.4570		

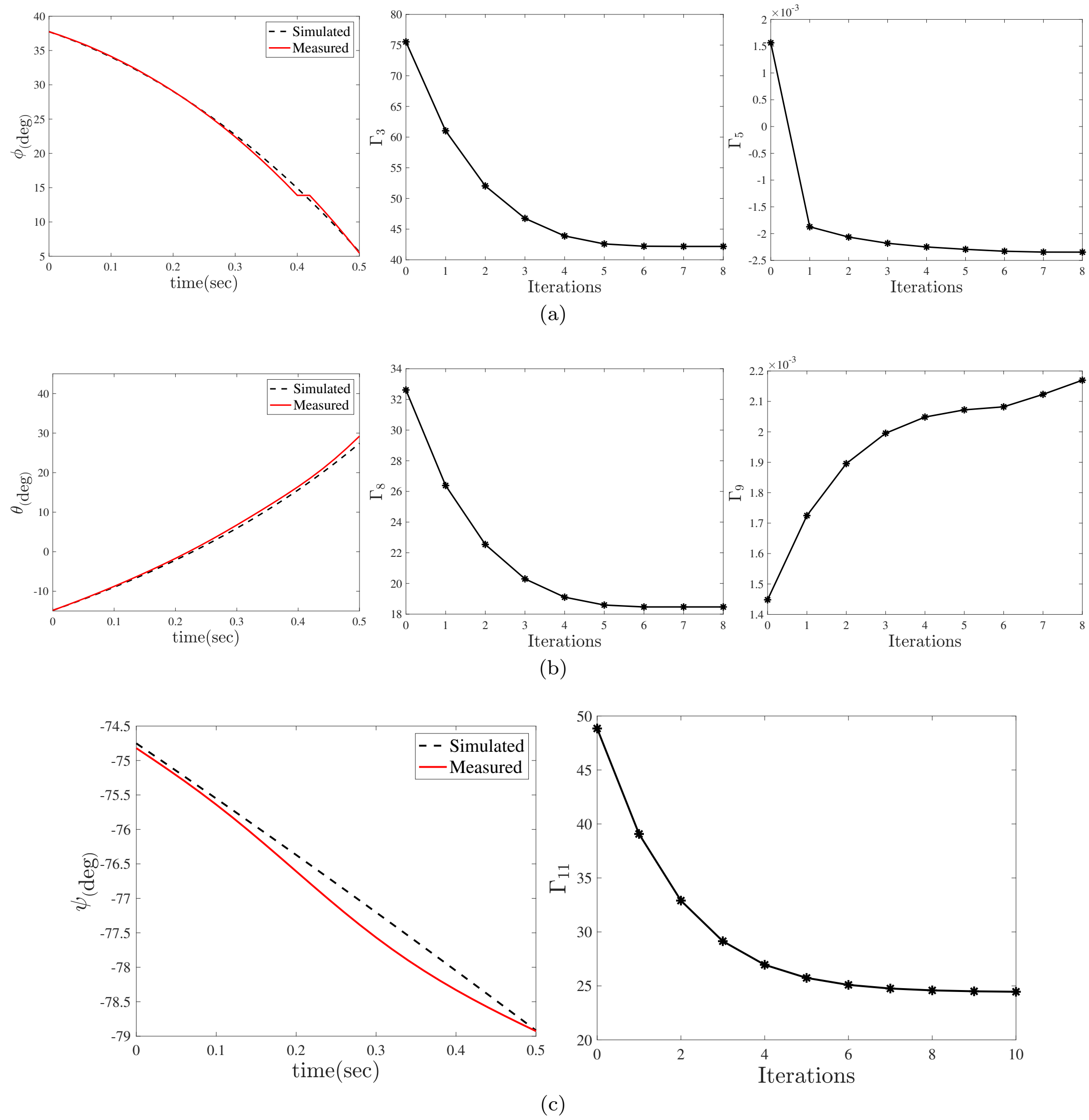

Figure 5: Identification process results when the quadrotor rotates about only one axis: (a) identification of Γ_3 and Γ_5 in free roll motion. (b) identification of Γ_8 and Γ_9 in free pitch motion. (c) identification of Γ_{11} in free yaw motion.

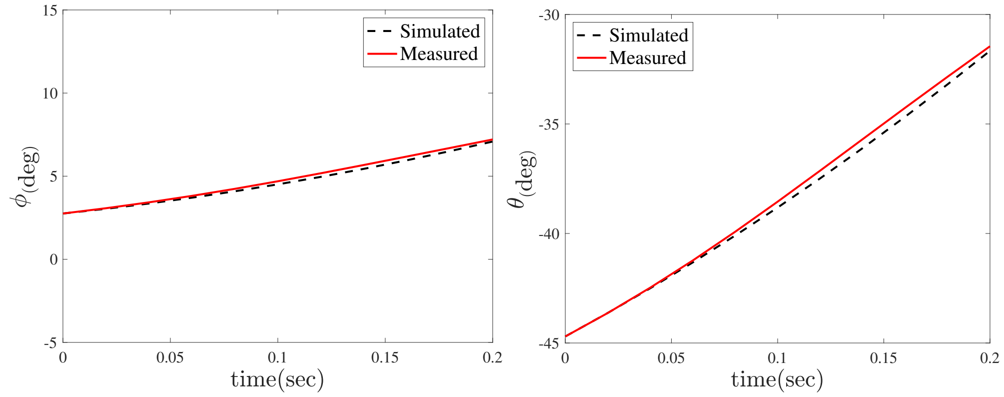

(a)

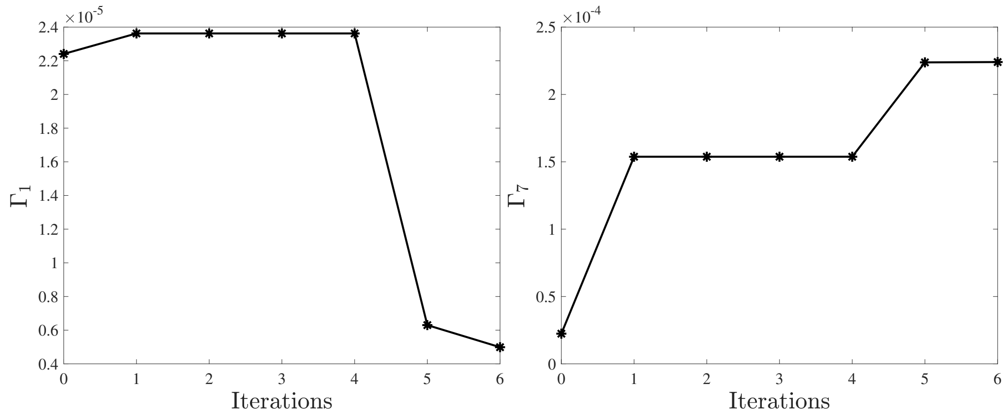

(b)

Figure 6: Identification process results when the quadrotor rotates about its roll and pitch axes: (a) comparison of simulation and experimental results. (b) identification of Γ_1 and Γ_7.

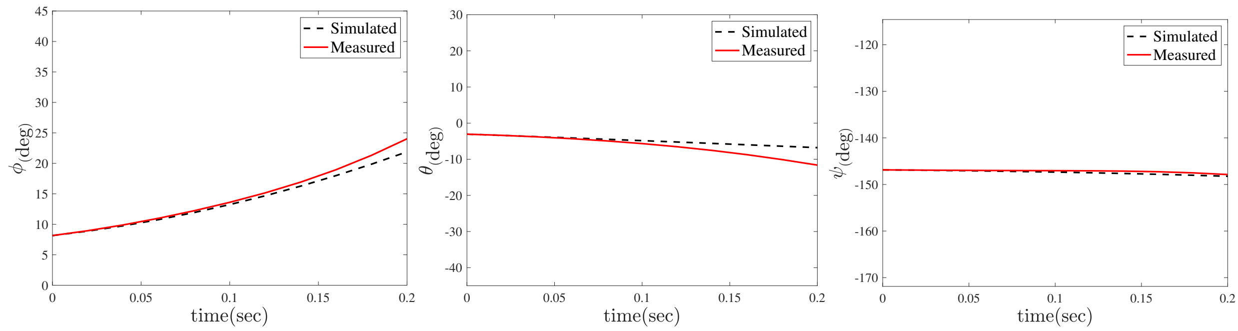

(a)

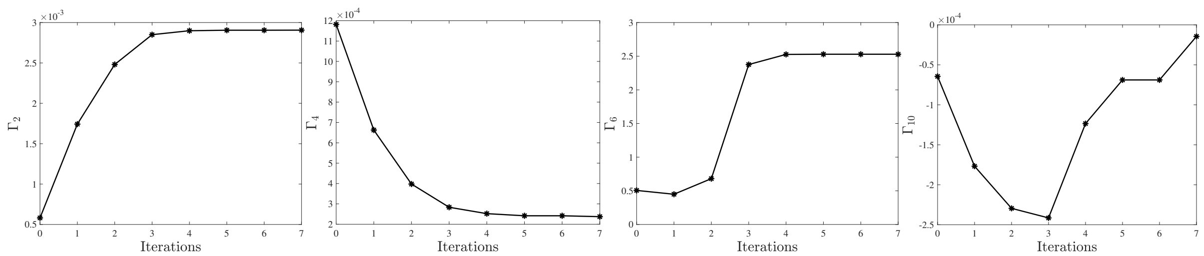

(b)

Figure 7: Identification process results when the quadrotor rotates about its roll, pitch, and yaw axes: (a) comparison of simulation and experimental results. (b) identification of Γ_2, Γ_4, Γ_6, and Γ_{10} parameters.

5.3. *Evaluation of LQIR-DG Performance*

In this section, the LQIR-DG controller algorithm is evaluated in three scenarios i) regulation and tracking problems, ii) disturbance rejection, and iii) impact of model uncertainty. Finally, a comparison of the proposed controller is performed with a PID controller and variants of the LQR controller. The PID controller parameters are presented in Table 6.

Table 6: PID controller parameters

Channel	K_p	K_i	K_d
roll	18	6	9
pitch	22	15	16

5.3.1. *Investigating of the Regulation and Tracking Problems*

The results of the proposed approach are presented for tracking the desired roll and pitch angles in Figures 8 and 9. Figure 8 (a) compares the desired and output signals, i.e., the Euler angles during the regulation problem. Moreover, Figure 8 (b) compares the desired square wave signals with a frequency of 0.02 Hz and an amplitude of 20 degrees with the output signals, when the quadrotor platform freely rotates around roll and pitch, simultaneity. Figures 9 (a) and (b) show the rotational velocity commands of the quadrotor in the regulation and tracking problems, respectively. These results demonstrate that the roll and pitch angles are accurately controlled by the proposed approach.

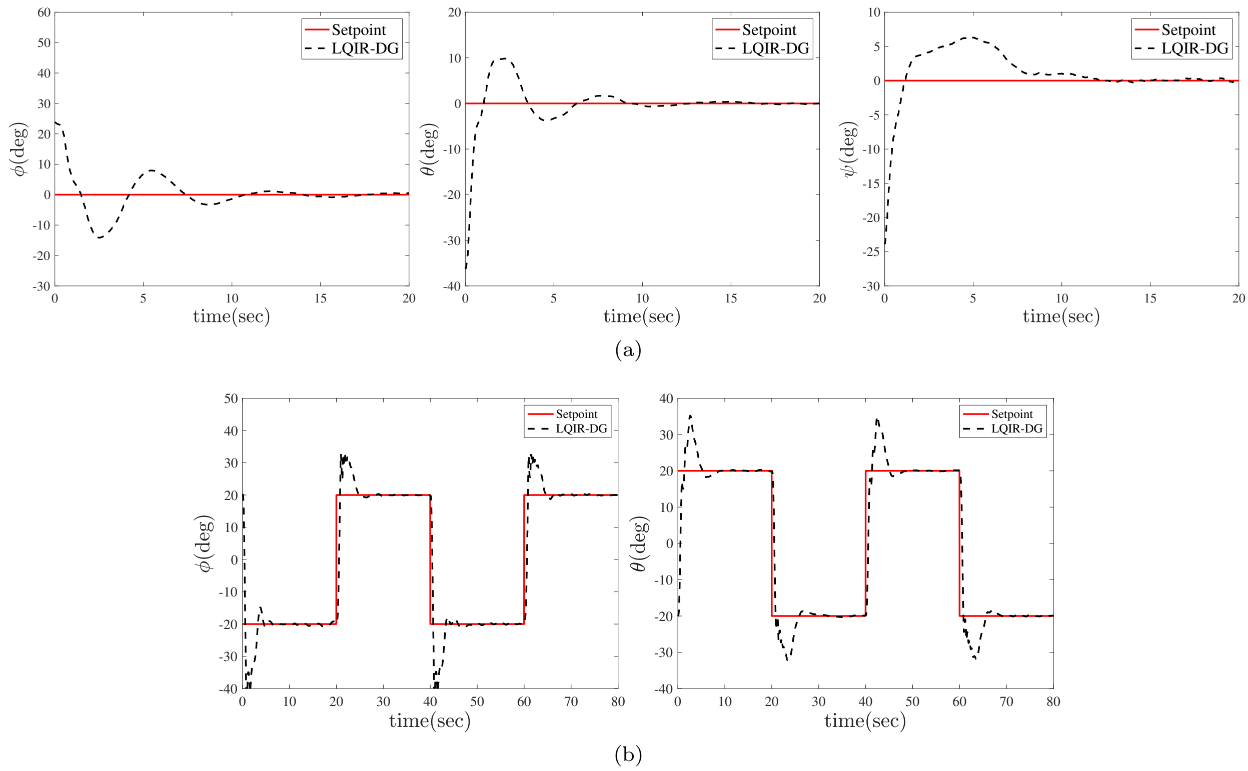

Figure 8: Comparison of actual roll and pitch angles with the desired values in (a) regulation and (b) tracking problems.

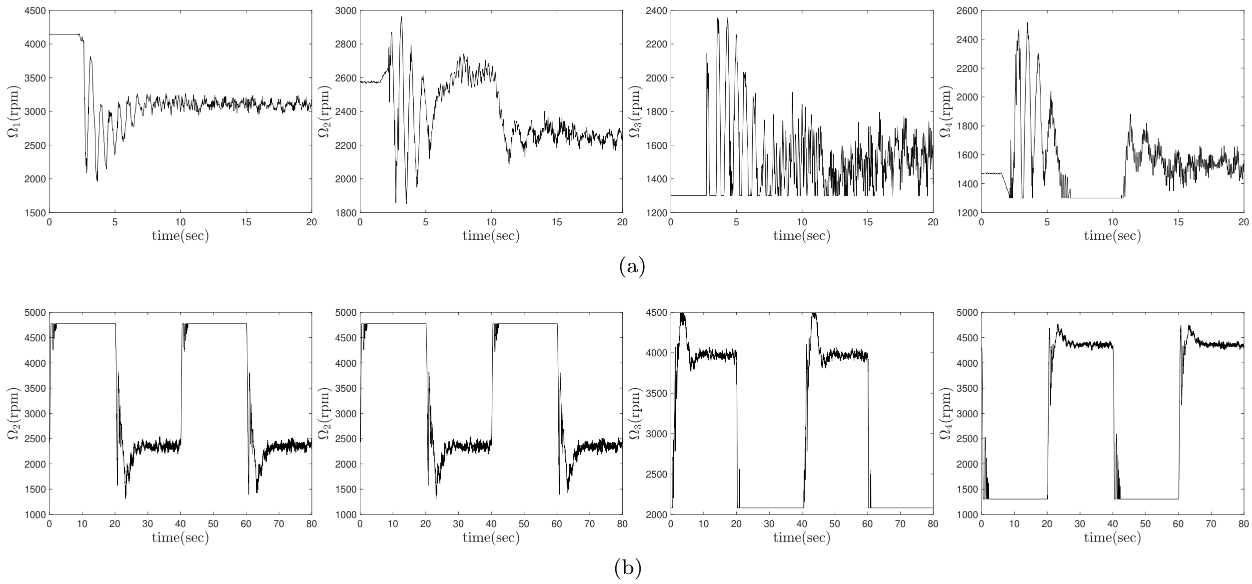

Figure 9: Rotational velocity commands in (a) regulation and (b) tracking problems.

5.3.2. Investigating the Disturbance Rejection

Here, the effect of the input disturbance is investigated on the performance of the proposed controller. The input disturbance, d_{Ω_i}, is considered as a change in command of the rotational velocity, modeled as

$$\mathrm{d}_{\Omega_1} = \mathrm{d}_{\Omega_2} = -\mathrm{d}_{\Omega_3} = -\mathrm{d}_{\Omega_4} = \begin{cases} 500 \text{ rpm} & 20 < t < 60 \\ 0 & \text{otherwise} \end{cases} \tag{29}$$

Figure 10 illustrates the roll and pitch angles in the regulation problem when the input disturbance occurs. These results indicate that the proposed controller can stabilize the quadrotor platform in the presence of input disturbance.

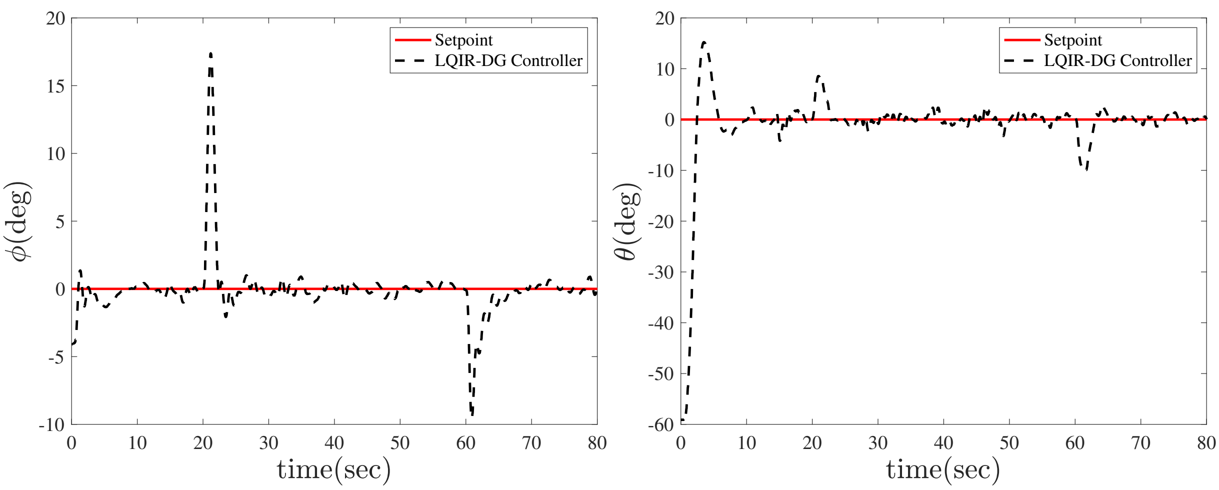

Figure 10: Comparison of actual roll and pitch angles with the desired, when the input disturbance occurs.

5.3.3. Investigating the Impact of Modeling Uncertainty

The effect of the modeling uncertainty is investigated on the performance of the proposed controller. To achieve this, 50 and 100 grams weights are added to the roll and pitch axes, respectively, as shown in Figure 11. Figure 12 (a) compares the desired and the actual roll angle and Figure 12 (b) shows the desired and the actual pitch angle, when the uncertainty of moments of inertia is present. Moreover, Figure 12 (c) shows the rotational velocity commands of the experimental platform, when the model uncertainty is applied. The implementation results show that the platform outputs converge to the desired values in the presence of the modeling uncertainty.

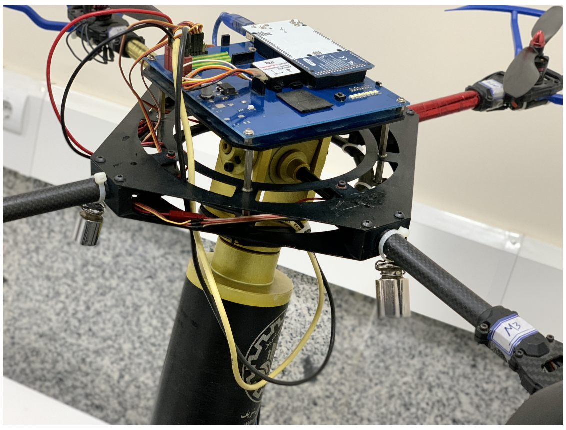

Figure 11: Quadrotor 3-DoF platform with added weights.

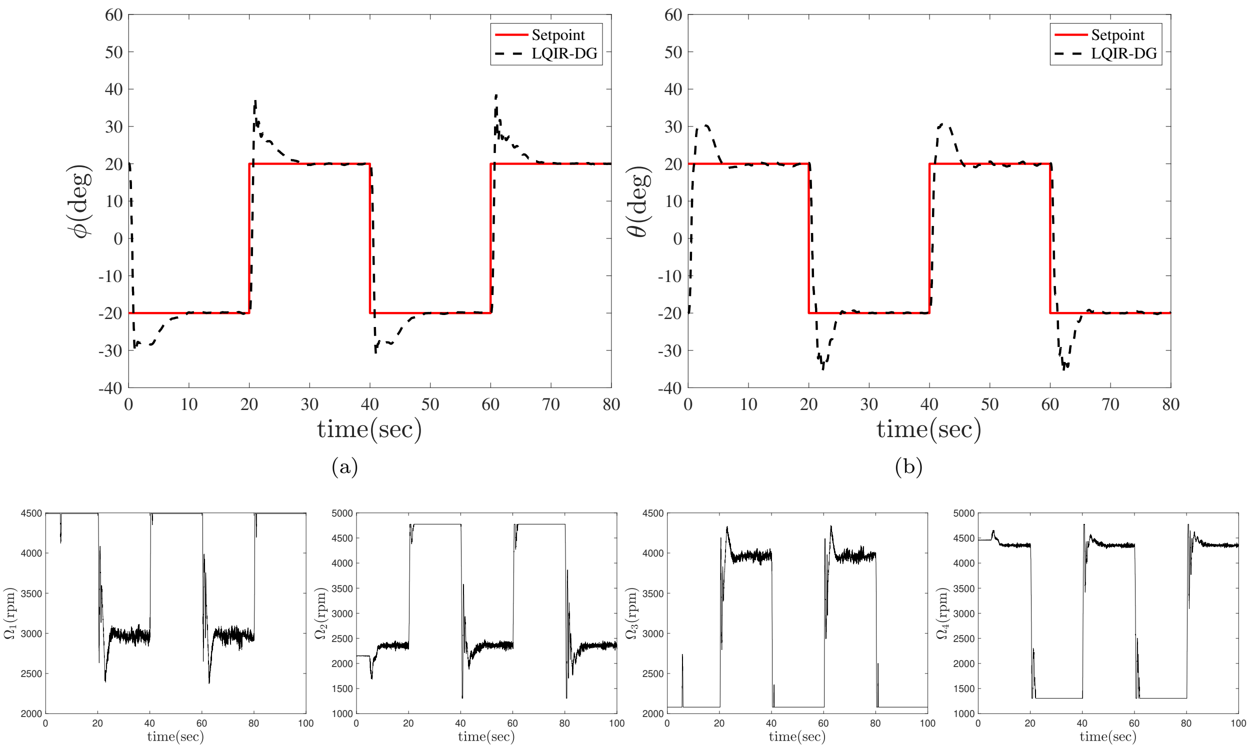

(a) (b)

(c)

Figure 12: Comparison of actual roll and pitch angles with desired values, when the modeling uncertainty is present.

5.3.4. Comparison with the Control Strategies

Figure 13 compares the LQIR-DG controller performance with the PID controller and variant of the LQR strategies such as the LQR and LQIR. Moreover, the box plot of all controllers is plotted in Figure 14 for the cost function, introduced in equation (22). The median of Root Mean Square Error (RMSE) is shown in the crossline in the box plot. Moreover, the LQIR-DG controller performance with famous disturbance rejection methods, such as Active Disturbance Rejection Control (ADRC) [8] and Disturbance Observer-Based Control (DOBC) [2] are compared in Figure 15, when the input disturbances occur according to equation (29). For the cost function, denoted in equation (22), the box plot of these robust controllers is illustrated in Figure 16. These results indicate that the proposed controller is able to provide rapid convergence, excellent transient, and robustness to disturbances relative to other controllers for attitude control of the experimental platform.

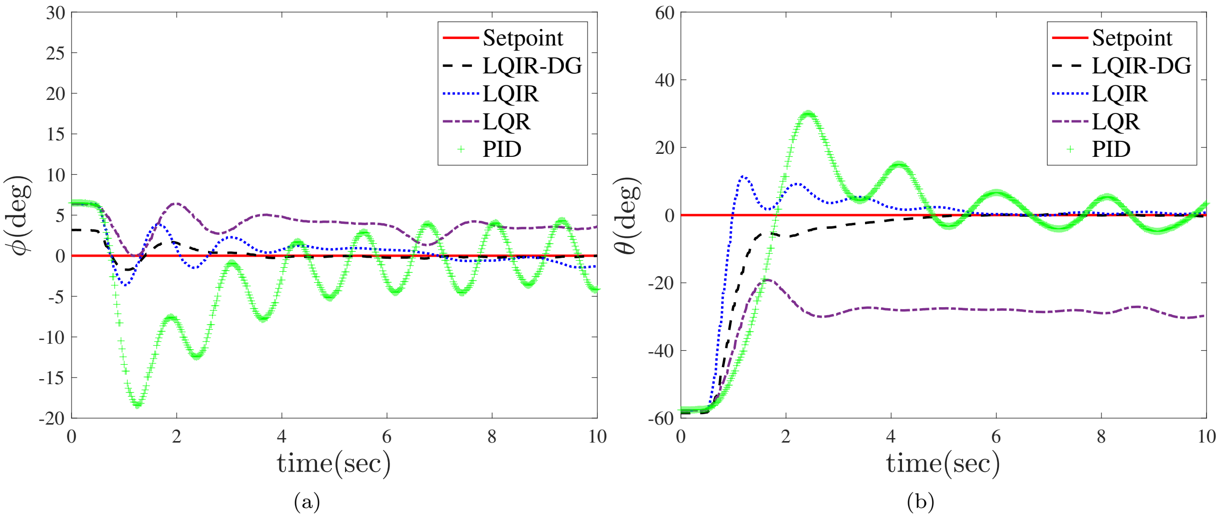

Figure 13: Comparison of LQIR-DG structure with the variant of LQR and PID in regulation problem: (a) roll angle (b) pitch angle.

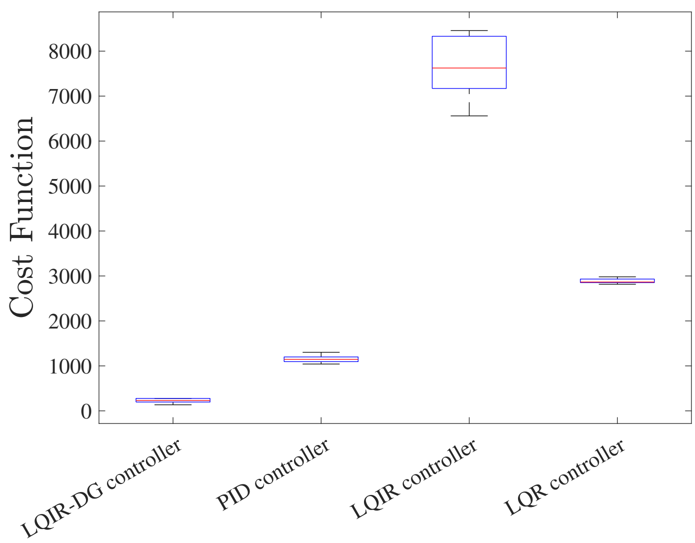

Figure 14: Box plot of LQIR-DG, LQR, LQIR, and PID controllers.

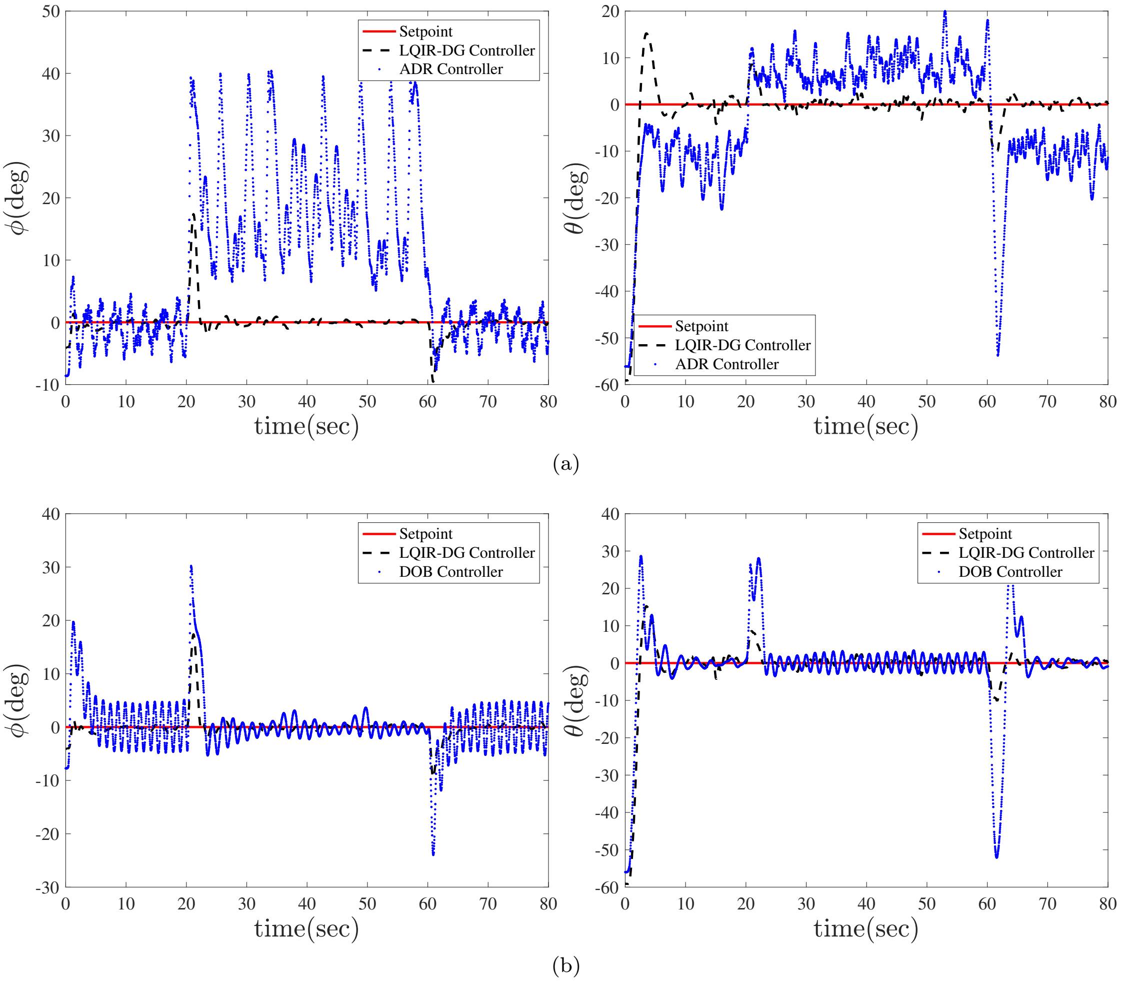

Figure 15: Comparison of LQIR-DG structure with the famous disturbance rejection methods: (a) Active Disturbance Rejection Control (ADRC) (b) Disturbance Observer-Based Control (DOBC).

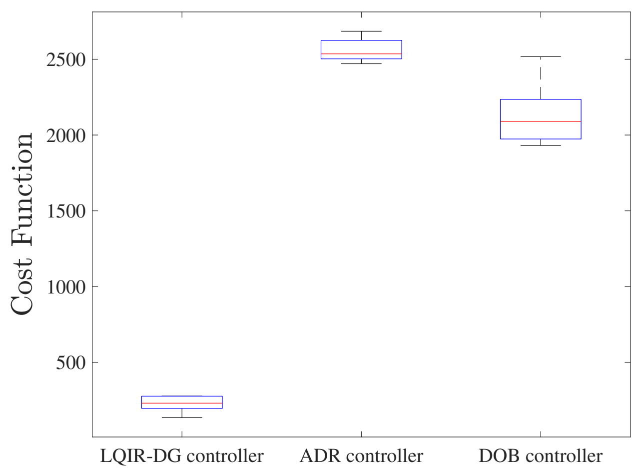

Figure 16: Box plot of LQIR-DG, ADRC, and DOBC methods.

6. Conclusion

In this paper, the linear quadratic integral differential game approach, was used in real-time for attitude control of the platform quadrotor. For the implementation of the controller structure, an accurate dynamic model was considered for the experimental platform. Then, the model parameters were identified using the NSL method. For evaluation of the proposed method, the regulation and tracking proposed were successfully performed. Moreover, the ability of the proposed method was investigated in the rejection of the input disturbance and modeling error in the experimental platform. Finally, a comparison was also performed between the results of classical PID variations of LQR and the robust structures with the proposed method. The implementation results illustrated the excellent performance of the LQIR controller based on the game theory approach in attitude control for the quadrotor platform. However, one challenge in applying this method to the 3-DOF quadrotor experimental setup was the presence of noise and errors of the AHRS sensor. It was calibrated before a run of the algorithm. One another challenge was in implementing the controller. Since, this controller required a desired trajectory, it was programmed on the Arduino Mega2560 board using the embedded coder before a run of the algorithm.

References

[1] Abdul Salam, A., Ibraheem, I., 2019. Nonlinear pid controller design for a 6-dof uav quadrotor system. Engineering Science and Technology, an International Journal 22. doi:10.1016/j.jestch.2019.02.005.

[2] Aghayan, Z.S., Alfi, A., Lopes, A.M., 2023. Disturbance observer-based delayed robust feedback control design for a class of uncertain variable fractional-order systems: Order-dependent and delay-dependent stability. ISA Transactions 138, 20–36. URL: https://www.sciencedirect.com/science/article/pii/S0019057823001052, doi:https://doi.org/10.1016/j.isatra.2023.03.008.

[3] Ahmad, F., Kumar, P., Bhandari, A., Patil, P.P., 2020. Simulation of the quadcopter dynamics with lqr based control. Materials Today: Proceedings 24, 326–332. URL: https://www.sciencedirect.com/science/article/pii/S2214785320329047, doi:https://doi.org/10.1016/j.matpr.2020.04.282. international Conference on Advances in Materials and Manufacturing Applications, IConAMMA 2018, 16th -18th August, 2018, India.

[4] Anjali, B., A., V., J L, N., 2016. Simulation and analysis of integral lqr controller for inner control loop design of a fixed wing micro aerial vehicle (mav). Procedia Technology 25, 76–83. doi:10.1016/j.protcy.2016.08.083.

[5] Bolandi, H., Rezaei, M., Mohsenipour, R., Nemati, H., Smailzadeh, S., 2013. Attitude control of a quadrotor with optimized pid controller. Intelligent Control and Automation 04, 342–349. doi:10.4236/ica.2013.43040.

[6] Bouabdallah, S., 2007. Design and control of quadrotors with application to autonomous flying. URL: https://api.semanticscholar.org/CorpusID:108233951.

[7] Bouabdallah, S., Siegwart, R., 2007. Full control of a quadrotor, in: 2007 IEEE/RSJ International Conference on Intelligent Robots and Systems, pp. 153–158. doi:10.1109/IROS.2007.4399042.

[8] Cheng, Y., Fan, Y., Zhang, P., Yuan, Y., Li, J., 2023. Design and parameter tuning of active disturbance rejection control for uncertain multivariable systems via quantitative feedback theory. ISA Transactions URL: https://www.sciencedirect.com/science/article/pii/S0019057823002926, doi:https://doi.org/10.1016/j.isatra.2023.06.025.

[9] Cortés-Romero, J., Delgado-Aguilera, E., Jimenez-Triana, A., 2020. Robust fractional active disturbance rejection control: A unified approach. ISA Transactions 107, 63–77. URL: https://www.sciencedirect.com/science/article/pii/S0019057820303268, doi:https://doi.org/10.1016/j.isatra.2020.08.003.

[10] Ding, R., Ding, C., Xu, Y., Liu, W., Yang, X., 2022. Neural network-based robust integral error sign control for servo motor systems with enhanced disturbance rejection performance. ISA Transactions 129, 580–591. URL: https://www.sciencedirect.com/science/article/pii/S0019057821006431, doi:https://doi.org/10.1016/j.isatra.2021.12.026.

[11] Elkhatem, A., Engin, S., 2021. Robust lqr and lqr-pi control strategies based on adaptive weighting matrix selection for a uav position and attitude tracking control. Alexandria Engineering Journal 61. doi:10.1016/j.aej.2021.11.057.

[12] Engwerda, J., 2005. LQ Dynamic Optimization and Differential Games.

[13] Engwerda, J., 2006. Linear Quadratic Games: An Overview. WorkingPaper. Macroeconomics. Subsequently published in Advances in Dynamic Games and their Applications (book), 2009 Pagination: 32.

[14] Foudeh, H.A., Luk, P., Whidborne, J., 2020. Application of norm optimal iterative learning control to quadrotor unmanned aerial vehicle for monitoring overhead power system. Energies 13. URL: https://www.mdpi.com/1996-1073/13/12/3223, doi:10.3390/en13123223.

[15] Glida, H.E., Chelihi, A., Abdou, L., Sentouh, C., Perozzi, G., 2022. Trajectory tracking control of a coaxial rotor drone: Timedelay estimation-based optimal modelfree fuzzy logic approach. ISA Transactions URL: https://www.sciencedirect.com/science/article/pii/S0019057822006462, doi:https://doi.org/10.1016/j.isatra.2022.12.015.

[16] Hwangbo, J., Sa, I., Siegwart, R., Hutter, M., 2017. Control of a quadrotor with reinforcement learning. IEEE Robotics and Automation Letters 2, 2096–2103. URL: https://doi.org/10.1109%2Flra.2017.2720851, doi:10.1109/lra.2017.2720851.

[17] Jin, X.Z., He, T., Wu, X.M., Wang, H., Chi, J., 2020. Robust adaptive neural network-based compensation control of a class of quadrotor aircrafts. Journal of the Franklin Institute 357, 12241–12263. URL: https://www.sciencedirect.com/science/article/pii/S0016003220306281, doi:https://doi.org/10.1016/j.jfranklin.2020.09.009.

[18] Karimi, A., Nobahari, H., Siarry, P., 2010. Continuous ant colony system and tabu search algorithms hybridized for global minimization of continuous multi-minima functions. Computational Optimization and Applications 45, 639–661. doi:10.1007/s10589-008-9176-7.

[19] Kirk, D., 2004. Optimal Control Theory: An Introduction. Dover Books on Electrical Engineering Series, Dover Publications. URL: https://books.google.nl/books?id=fCh2SAtWIdwC.

[20] Labbadi, M., Cherkaoui, M., 2020. Robust adaptive nonsingular fast terminal sliding-mode tracking control for an uncertain quadrotor uav subjected to disturbances. ISA Transactions 99, 290–304. URL: https://www.sciencedirect.com/science/article/pii/S0019057819304665, doi:https://doi.org/10.1016/j.isatra.2019.10.012.

[21] Lin, X., Liu, J., Yu, Y., Sun, C., 2020. Event-triggered reinforcement learning control for the quadrotor uav with actuator saturation. Neurocomputing 415, 135–145. URL: https://www.sciencedirect.com/science/article/pii/S0925231220311504, doi:https://doi.org/10.1016/j.neucom.2020.07.042.

[22] Miranda-Colorado, R., Aguilar, L.T., 2020. Robust pid control of quadrotors with power reduction analysis. ISA Transactions 98, 47–62. URL: https://www.sciencedirect.com/science/article/pii/S001905781930391X, doi:https://doi.org/10.1016/j.isatra.2019.08.045.

[23] Mofid, O., Mobayen, S., Zhang, C., Esakki, B., 2022. Desired tracking of delayed quadrotor uav under model uncertainty and wind disturbance using adaptive super twisting terminal sliding mode control. ISA Transactions 123. URL: https://www.sciencedirect.com/science/article/pii/S0019057821003086, doi:https://doi.org/10.1016/j.isatra.2021.06.002.

[24] Rekabi, F., Shirazi, F.A., Sadigh, M.J., 2020. Distributed nonlinear h_∞ control algorithm for multi-agent quadrotor formation flying. ISA Transactions 96, 81–94. URL: https://www.sciencedirect.com/science/article/pii/S001905781930165X, doi:https://doi.org/10.1016/j.isatra.2019.04.036.

[25] Rodríguez-Martínez, G., Romero, J.G., Mosco-Luciano, A., Rodríguez-Cortés, H., 2023. Asymptotic stabilization of a transformed quadrotor model using energy-shaping method: Theory and experiments. ISA Transactions 139, 739–749. URL: https://www.sciencedirect.com/science/article/pii/S0019057823002033, doi:https://doi.org/10.1016/j.isatra.2023.04.034.

[26] Santos, D.A., Lagoa, C.M., 2022. Wayset-based guidance of multirotor aerial vehicles using robust tube-based model predictive control. ISA Transactions 128, 123–135. URL: https://www.sciencedirect.com/science/article/pii/S0019057821006182, doi:https://doi.org/10.1016/j.isatra.2021.12.002.

[27] Simon, D., 2006. Optimal State Estimation: Kalman, H Infinity, and Nonlinear Approaches. Wiley-Interscience, 605 Third Avenue, New York, NY, United States.

[28] de Souza Câmara, R.G., Santos, T.L.M., 2023. Robust decoupling mpc for linear systems with bounded disturbances. ISA Transactions 139, 1–12. URL: https://www.sciencedirect.com/science/article/pii/S0019057823002215, doi:https://doi.org/10.1016/j.isatra.2023.05.004.

[29] Wang, H., Li, Z., Xiong, H., Nian, X., 2019. Robust h_∞ attitude tracking control of a quadrotor uav on so(3) via variation-based linearization and interval matrix approach. ISA Transactions 87, 10–16. URL: https://www.sciencedirect.com/science/article/pii/S0019057818304518, doi:https://doi.org/10.1016/j.isatra.2018.11.015.

[30] Wang, Y., Liu, W., Liu, J., Sun, C., 2023. Cooperative usv-uav marine search and rescue with visual navigation and reinforcement learning-based control. ISA Transactions 137, 222–235. URL: https://www.sciencedirect.com/science/article/pii/S0019057823000071, doi:https://doi.org/10.1016/j.isatra.2023.01.007.

[31] Wei, W., Duan, B., Zhang, W., Zuo, M., 2022. Active disturbance rejection control for nanopositioning: A robust u-model approach. ISA Transactions 128, 599–610. URL: https://www.sciencedirect.com/science/article/pii/S0019057821006066, doi:https://doi.org/10.1016/j.isatra.2021.11.035.

[32] Wu, X., Xiao, B., Qu, Y., 2022. Modeling and sliding mode-based attitude tracking control of a quadrotor uav with time-varying mass. ISA Transactions 124, 436–443. URL: https://www.sciencedirect.com/science/article/pii/S0019057819303544, doi:https://doi.org/10.1016/j.isatra.2019.08.017.

[33] Xu, Q., Wang, Z., Zhen, Z., 2020. Information fusion estimation-based path following control of quadrotor uavs subjected to gaussian random disturbance. ISA Transactions 99, 84–94. URL: https://www.sciencedirect.com/science/article/pii/S0019057819304574, doi:https://doi.org/10.1016/j.isatra.2019.10.003.

[34] Yan, D., Zhang, W., Chen, H., Shi, J., 2023. Robust control strategy for multi-uavs system using mpc combined with kalman-consensus filter and disturbance observer. ISA Transactions 135, 35–51. URL: https://www.sciencedirect.com/science/article/pii/S0019057822004797, doi:https://doi.org/10.1016/j.isatra.2022.09.021.

[35] Yang, X., Yao, J., Deng, W., 2021. Output feedback adaptive super-twisting sliding mode control of hydraulic systems with disturbance compensation. ISA Transactions 109, 175–185. URL: https://www.sciencedirect.com/science/article/pii/S0019057820303888, doi:https://doi.org/10.1016/j.isatra.2020.09.014.

[36] Zulu, A., John, S., 2014. A review of control algorithms for autonomous quadrotors. Open Journal of Applied Sciences 04, 547–556. doi:10.4236/ojapps.2014.414053.

[37] Zwierzewicz, Z., 2014. On the ship course-keeping control system design by using robust and adaptive control, in: 2014 19th International Conference on Methods and Models in Automation and Robotics (MMAR), pp. 189–194. doi:10.1109/MMAR.2014.6957349.

Appendix A. Linearization Proof of the Quadrotor Nonlinear Model

Here, the nonlinear model of the quadrotor, described in equations (10)-(15), are linearized using first-order Taylor series expansion about the equilibrium points ($\boldsymbol{x}^*$ and $\boldsymbol{u}^*$). For this purpose, the linear form of the nonlinear system denoted as $\dot{\boldsymbol{x}} = \boldsymbol{f}(\boldsymbol{x}, \boldsymbol{u})$, is computed as

$$\dot{\boldsymbol{x}} = \mathbf{A}\boldsymbol{x} + \mathbf{B}\boldsymbol{u} \tag{A.1}$$

where $\mathbf{A}$ and $\mathbf{B}$ are, respectively, the states and input matrices, computed as [27]

$$\mathbf{A} = \left.\frac{\partial \mathbf{f}}{\partial \mathbf{x}}\right|_{\mathbf{x}^*, \mathbf{u}^*} \tag{A.2}$$

$$\mathbf{B} = \left.\frac{\partial \mathbf{f}}{\partial \mathbf{u}}\right|_{\mathbf{x}^*, \mathbf{u}^*} \tag{A.3}$$

To linearize the nonlinear model of the quadrotor around the equilibrium points ($\boldsymbol{x}^* = 0$ and $\boldsymbol{u}^* = 0$), the Jacobian matrix of nonlinear model, denoted in equations (10)-(15), is expressed as:

$$\mathbf{A} = \left.\frac{\partial \mathbf{f}}{\partial \mathbf{x}}\right|_{\mathbf{x}^* = \mathbf{u}^* = \mathbf{0}} = \begin{bmatrix} \frac{\partial f_1}{\partial x_1} & \cdots & & \cdots & \frac{\partial f_1}{\partial x_6} \\ \vdots & \ddots & & & \vdots \\ & & \ddots & & \\ \frac{\partial f_4}{\partial x_1} & \cdots & \frac{\partial f_4}{\partial x_4} & \cdots & \frac{\partial f_4}{\partial x_6} \\ \vdots & & & \ddots & \vdots \\ \frac{\partial f_6}{\partial x_1} & \cdots & & \cdots & \frac{\partial f_6}{\partial x_6} \end{bmatrix} \tag{A.4}$$

$$= \begin{bmatrix} \Gamma_1 x_3 & 0 & -\Gamma_2 x_5 & 0 & -\Gamma_2 x_3 & 0 \\ 1 & a_{21} & \sin(x_2)\tan(x4) & a_{24} & \cos(x_2)\tan(x4) & 0 \\ a_{31} & 0 & 0 & 0 & \Gamma_6 x_1 + 2\Gamma_7 x_5 & 0 \\ 0 & -x_3\sin(x_2) - x_5\cos(x_2) & \cos(x_2) & 0 & -\sin(x_2) & 0 \\ \Gamma_{10} x_3 & 0 & \Gamma_{10} x_1 - \Gamma_1 x_5 & 0 & -\Gamma_1 x_3 & 0 \\ 0 & \frac{x_3\cos(x_2) - x_5\sin(x_2)}{\cos(x_4)} & \frac{\sin(x_2)}{\cos(x_4)} & a_{64} & \frac{\cos(x_2)}{\cos(x_4)} & 0 \end{bmatrix} \tag{A.5}$$

Here, $a_{21} = (x_3\cos(x_2) - x_5\sin(x_2))\tan(x_4)$, $a_{24} = (x_3\sin(x_2) + x_5\cos(x_2))\sec^2(x_4)$, $a_{31} = \Gamma_6 x_5 - 2\Gamma_7 x_1$, and $a_{64} = x_3 + \sin(x_4)(x_5\cos(x_2) + x_3\sin(x_4))\sec(x_4)^2$.

$$\mathbf{B} = \left.\frac{\partial \mathbf{f}}{\partial \mathbf{u}}\right|_{\mathbf{x}^* = \mathbf{u}^* = \mathbf{0}} = \begin{bmatrix} \frac{\partial f_1}{\partial u_{\text{roll}}} & \frac{\partial f_1}{\partial u_{\text{pitch}}} & \frac{\partial f_1}{\partial u_{\text{yaw}}} \\ \vdots & \vdots & \vdots \\ \frac{\partial f_6}{\partial u_{\text{roll}}} & \frac{\partial f_6}{\partial u_{\text{pitch}}} & \frac{\partial f_6}{\partial u_{\text{yaw}}} \end{bmatrix} = \begin{bmatrix} \Gamma_3 & 0 & \Gamma_4 \\ 0 & 0 & 0 \\ 0 & \Gamma_8 & 0 \\ 0 & 0 & 0 \\ \Gamma_4 & 0 & \Gamma_{11} \\ 0 & 0 & 0 \end{bmatrix} \tag{A.6}$$

Finally, the linearized matrices, defined at the equilibrium points, are given as:

$$\mathbf{A} = \frac{\partial \mathbf{f}}{\partial \mathbf{x}}\bigg|_{\mathbf{x}_e^*,\mathbf{u}_e^*} = \begin{bmatrix} 0 & 0 & 0 & 0 & 0 & 0 \\ 1 & 0 & 0 & 0 & 0 & 0 \\ 0 & 0 & 0 & 0 & 0 & 0 \\ 0 & 0 & 1 & 0 & 0 & 0 \\ 0 & 0 & 0 & 0 & 0 & 0 \\ 0 & 0 & 0 & 0 & 1 & 0 \end{bmatrix} \tag{A.7}$$

$$\mathbf{B} = \frac{\partial \mathbf{f}}{\partial \mathbf{u}}\bigg|_{\mathbf{x}_e^*,\mathbf{u}_e^*} = \begin{bmatrix} \Gamma_3 & 0 & \Gamma_4 \\ 0 & 0 & 0 \\ 0 & \Gamma_8 & 0 \\ 0 & 0 & 0 \\ \Gamma_4 & 0 & \Gamma_{11} \\ 0 & 0 & 0 \end{bmatrix} \tag{A.8}$$

Appendix B. Proof of the LQIR-DG controller

Since, the first player determines the control commands and second player generates the worst possible disturbance, a performance index of the differential game [12], described by equation (22), is rearranged as

$$\max_{d_i} \min u_i J(\mathbf{x}_{\mathrm{a}_i}, d_i, u_i) = \min_{d_i} (-J(\mathbf{x}_{_i}, d_i, u_i)) \min_{u_i} J(\mathbf{x}_{\mathrm{a}_i}, d_i, u_i) \tag{B.1}$$

that are subjected to the augmented system, denoted in equation (21). To find the optimal control policy function, u_i, it is assumed that the solution for the above optimization problem is unique and $d_i = \mathbf{K}_{d_i}\mathbf{x}_{\mathrm{a}_1}$. Moreover, Pontryagin's maximum principle [19] is utilized to minimize the following Hamiltonian related to the first player

$$\mathcal{H}_1 = \frac{1}{2}\mathbf{x}_{\mathrm{a}_i}^{\mathrm{T}}\mathbf{Q}\mathbf{x}_{\mathrm{a}_i} + \frac{1}{2}\mathbf{u}_i^{\mathrm{T}} R \mathbf{u}_i - \frac{1}{2}\mathbf{x}_{\mathrm{a}_i}^{\mathrm{T}}\mathbf{K}_{d_i} R_d \mathbf{K}_{d_i}\mathbf{x}_{\mathrm{a}_i} + \lambda_1^{\mathrm{T}}(\mathbf{A}\mathbf{x}_{\mathrm{a}_i} + \mathbf{B}_{\mathrm{a}_i}\mathbf{u}_i + \mathbf{B}_{\mathrm{a}_i}\mathbf{K}_{d_i}\mathbf{x}_{\mathrm{a}_i}) \tag{B.2}$$

where λ_1 is the Lagrangian variable related to the first player. Hence, the first-order necessary conditions for a minimize of this Hamiltonian are given by

$$\frac{\partial \mathcal{H}_1}{\partial u_i} = 0 \Rightarrow R u_i + \mathbf{B}_{\mathrm{a}_i}^{\mathrm{T}}\lambda_1 = 0 \Rightarrow u_i = -R^{-1}\mathbf{B}_{\mathrm{a}_i}^{\mathrm{T}}\lambda_1 \tag{B.3}$$

$$\dot{\lambda}_1 = -\frac{\partial \mathcal{H}_1}{\partial \mathbf{x}_{\mathrm{a}_i}} = -(\mathbf{Q}_i - \mathbf{K}_{d_i}^{\mathrm{T}} R_d \mathbf{K}_{d_i} - \lambda_1^{\mathrm{T}}(\mathbf{A}_{\mathrm{a}_i} + \mathbf{B}_{\mathrm{a}_i}\mathbf{K}_{d_i}))\mathbf{x}_{\mathrm{a}_i} \tag{B.4}$$

$$\dot{\mathbf{x}}_{\mathrm{a}_i} = \frac{\partial \mathcal{H}_1}{\partial \lambda_1} = \mathbf{A}_{\mathrm{a}_i}\mathbf{x}_{\mathrm{a}_i} + \mathbf{B}_{\mathrm{a}_i}\mathbf{u}_i + \mathbf{B}_{\mathrm{a}_i}\mathbf{K}_{d_i}\mathbf{x}_{\mathrm{a}_i} \tag{B.5}$$

By assuming $\lambda_1 = \mathbf{P}_{\mathrm{a}_i}\mathbf{x}_{\mathrm{a}_i}$, $\dot{\mathbf{P}}_{\mathrm{a}_i} = 0$, and combining above equations, the Riccati equation for first player is obtained as follows:

$$-(\mathbf{A}_{\mathrm{a}_i} + \mathbf{B}_{\mathrm{a}_i}\mathbf{K}_{d_i})^{\mathrm{T}}\mathbf{P}_{\mathrm{a}_i} - \mathbf{P}_{\mathrm{a}_i}(\mathbf{A}_{\mathrm{a}_i} + \mathbf{B}_{\mathrm{a}_i}\mathbf{K}_{d_i}) + \mathbf{P}_{\mathrm{a}_i}\mathbf{B}_{\mathrm{a}_i}\mathbf{R}^{-1}\mathbf{B}_{\mathrm{a}_i}^{\mathrm{T}}\mathbf{P}_{\mathrm{a}_i} - \mathbf{Q}_{\mathrm{a}_i} + \mathbf{K}_{d_i}^{\mathrm{T}} R_d \mathbf{K}_{d_i} = 0 \tag{B.6}$$

Moreover, the optimal control is obtained as follows:

$$u_i = -\mathbf{R}^{-1}\mathbf{B}_{\mathrm{a}_i}^{\mathrm{T}}\mathbf{P}_{\mathrm{a}_i}\mathbf{x}_{\mathrm{a}_i} \tag{B.7}$$

Assume that $\mathbf{K}_{\mathrm{a}_i} = -R^{-1}\mathbf{B}_{\mathrm{a}_i}^{\mathrm{T}}\mathbf{P}_{\mathrm{a}_i}$, then $u_i = \mathbf{K}_{\mathrm{a}_i}\mathbf{x}_{\mathrm{a}_i}$. Similarly, the second player is obtained using the following Hamiltonian

$$\mathcal{H}_2 = -\frac{1}{2}\mathbf{x}_{\mathrm{a}_i}^{\mathrm{T}}\mathbf{Q}\mathbf{x}_{\mathrm{a}_i} - \frac{1}{2}\mathbf{u}_i^{\mathrm{T}} R \mathbf{u}_i + \frac{1}{2}\mathbf{x}_{\mathrm{a}_i}^{\mathrm{T}}\mathbf{K}_{d_i} R_d \mathbf{K}_{d_i}\mathbf{x}_{\mathrm{a}_i} + \lambda_1^{\mathrm{T}}(\mathbf{A}\mathbf{x}_{\mathrm{a}_i} + \mathbf{B}_{\mathrm{a}_i}\mathbf{u}_i + \mathbf{B}_{\mathrm{a}_i}\mathbf{K}_{d_i}\mathbf{x}_{\mathrm{a}_i}) \tag{B.8}$$

Here λ_2 is the Lagrangian variable related to the second player. Therefore, the necessary conditions for a maximum worst case are computed as

$$\frac{\partial \mathcal{H}_2}{\partial d_i} = 0 \Rightarrow R_d d_i + \mathbf{B}_{\mathrm{a}_i}^{\mathrm{T}} \lambda_2 = 0 \Rightarrow d_i = -R_d^{-1} \mathbf{B}_{\mathrm{a}_i}^{\mathrm{T}} \lambda_2 \tag{B.9}$$

$$\dot{\lambda}_2 = -\frac{\partial \mathcal{H}_2}{\partial \mathbf{x}_{\mathrm{a}_i}} = (\mathbf{Q}_i - \mathbf{K}_{d_i}^{\mathrm{T}} R \mathbf{K}_{d_i} - \lambda_2^{\mathrm{T}} (\mathbf{A}_{\mathrm{a}_i} + \mathbf{B}_{\mathrm{a}_i} \mathbf{K}_{d_i})) \mathbf{x}_{\mathrm{a}_i} \tag{B.10}$$

$$\dot{\mathbf{x}}_{\mathrm{a}_i} = \frac{\partial \mathcal{H}_2}{\partial \lambda_2} = \mathbf{A}_{\mathrm{a}_i} \mathbf{x}_{\mathrm{a}_i} + \mathbf{B}_{\mathrm{a}_i} \mathbf{K}_{d_i} \mathbf{x}_{\mathrm{a}_i} + \mathbf{B}_{\mathrm{a}_i} \mathbf{d}_i \tag{B.11}$$

By assuming $\lambda_2 = \mathbf{P}_{\mathrm{a}_{d_i}} \mathbf{x}_{\mathrm{a}_i}$, $\dot{\mathbf{P}}_{\mathrm{a}_{d_i}} = 0$, and combining equations (B.9), (B.10) and (B.11), the Riccati equation for first player is obtained as follows:

$$-(\mathbf{A}_{\mathrm{a}_i} + \mathbf{B}_{\mathrm{a}_i} \mathbf{K}_{\mathrm{a}_i})^{\mathrm{T}} \mathbf{P}_{\mathrm{a}_{d_i}} - \mathbf{P}_{\mathrm{a}_{d_i}} (\mathbf{A}_{\mathrm{a}_i} + \mathbf{B}_{\mathrm{a}_i} \mathbf{K}_{\mathrm{a}_i}) + \mathbf{P}_{\mathrm{a}_{d_i}} \mathbf{B}_{\mathrm{a}_i} \mathbf{R}_d^{-1} \mathbf{B}_{\mathrm{a}_i}^{\mathrm{T}} \mathbf{P}_{\mathrm{a}_{d_i}} + \mathbf{Q}_{\mathrm{a}_i} + \mathbf{K}_{\mathrm{a}_i}^{\mathrm{T}} R \mathbf{K}_{\mathrm{a}_i} = 0 \tag{B.12}$$

Moreover, the worst disturbance is obtained as follows:

$$d_i = -R_d^{-1} \mathbf{B}_{\mathrm{a}_i}^{\mathrm{T}} \mathbf{P}_{\mathrm{a}_{d_i}} \mathbf{x}_{\mathrm{a}_i} \tag{B.13}$$

Therefore, $\mathbf{K}_{\mathrm{d}_i} = -R_d^{-1} \mathbf{B}_{\mathrm{a}_i}^{\mathrm{T}} \mathbf{P}_{\mathrm{a}_{d_i}}$. By combining two Riccati equations ((B.6) and (B.12)), the following equation is computed:

$$-(\mathbf{P}_{\mathrm{a}_i} + \mathbf{P}_{\mathrm{a}_{d_i}}) (\mathbf{A}_{\mathrm{a}_i} - \mathbf{S}_{\mathrm{a}_i} \mathbf{P}_{\mathrm{a}_i} - \mathbf{S}_{\mathrm{a}_i} \mathbf{P}_{\mathrm{a}_i}) - (\mathbf{A}_{\mathrm{a}_i} - \mathbf{S}_{\mathrm{a}_i} \mathbf{P}_{\mathrm{a}_i} - \mathbf{S}_{\mathrm{a}_i} \mathbf{P}_{\mathrm{a}_i})^{\mathrm{T}} (\mathbf{P}_{\mathrm{a}_i} + \mathbf{P}_{\mathrm{a}_{d_i}}) = 0 \tag{B.14}$$

where $\mathbf{S}_{\mathrm{a}_i} = \mathbf{B}_{\mathrm{a}_i} R^{-1} \mathbf{B}_{\mathrm{a}_i}^{\mathrm{T}}$ and $\mathbf{S}_{\mathrm{a}_{\mathrm{d}\,i}} = \mathbf{B}_{\mathrm{a}_i} R_d^{-1} \mathbf{B}_{\mathrm{a}_i}^{\mathrm{T}}$. Therefore, $\mathbf{P}_{\mathrm{a}_i} = -\mathbf{P}_{\mathrm{a}_{d_i}}$ and two Ricatti equations have a following solution:

$$-\mathbf{A}_{\mathrm{a}_i}^{\mathrm{T}} \mathbf{P}_{\mathrm{a}_i} - \mathbf{P}_{\mathrm{a}_i} \mathbf{A}_{\mathrm{a}_i} + \mathbf{P}_{\mathrm{a}_i} (\mathbf{S}_{\mathrm{a}_i} - \mathbf{S}_{\mathrm{a}_{\mathrm{d}\,i}}) \mathbf{P}_{\mathrm{a}_i} - \mathbf{Q}_i = 0 \tag{B.15}$$